Relation of plasma flow structures to passive particle tracer orbits

L. García[1], B.A. Carreras[2] and I. Llerena[3]

[1] Departamento de Física, Universidad Carlos III de Madrid, Avda. de la Universidad 30, 28911 Leganés, Madrid, Spain
[2] BACV Solutions, 110 Mohawk Road, Oak Ridge, Tennessee 37830, USA
[3] Departament d'Àlgebra i Geometria, Facultat de Matemàtiques, Universitat de Barcelona, Gran Via de les Corts Catalanes, 585, 08007 Barcelona, Spain

E-mail: lgarcia@fis.uc3m.es, bacarreras@gmail.com and illerena@ub.edu

Abstract. The properties of plasma flow topological structures are compared with those of passive tracer particles within a framework of the continuous random walk (CTRW) approach. Vortices may cause some of the trapping of particles, while large scale flows may carry them from vortex to vortex. The results indicate that most of the trappings that are completed during the calculation correspond to tracers trapped on broken filaments, including possible multiple trappings. The probability distribution function of the trapping times is then a function of the filament length, and has a lognormal character, like the distribution of filament lengths.

PACS numbers: 52.35.Ra, 52.65.Kj, 47.27.-i

1. Introduction

Turbulence induced transport is one of the outstanding physics problems in plasma physics [1]. In the turbulence induced transport issue, we proceed in three steps. First, the identification of turbulent flow structures using topological and geometric techniques and characterization of their statistical properties [2, 3]. Second, to relate these topological structures to properties of passive tracer particles within a framework of the CTRW approach [4]. Third, to construct a transport theory based on the CTRW approach and use the information we obtained in characterizing the tracer particle properties. We are working on the framework of the Resistive Magnetohydrodynamic (MHD) turbulence and we are now at the second step in the process.

In the first step of our research, we used topological tools to characterize the flow structures [2, 3]. The main finding of Ref. [2] was that the structure of the flow is filamentary. The filaments are vortices that are linked to the rational surfaces, i.e. surfaces where the safety factor q (pitch of the magnetic field line) is a rational number m/n. Some of these filamentary vortices close on themselves forming toroidal knots and they are normally located at the rational surfaces where m and n have the lowest values. In this paper we call these structures cycles. At the other low rational surfaces the filaments are broken and we characterise them by their length.

The use of particle passive tracers has proven to be very helpful in trying to understand turbulence-induced transport in magnetically confined plasmas. Particle

tracers have been used in numerical simulations to characterize diffusive transport [5], [6], [7] and also non-diffusive transport [8]. Since we are interested in the radial transport, we look at the projection of the passive tracer trajectories on the radial direction. We use this approach and relate the tracer orbits to flow structures. To do so, we first decompose the tracer trajectories in radial flights and trappings. In a general way, flights can be defined as intervals of the orbits between points where the radial velocity changes sign. Then, we define as trapping a sequence of flights oscillating around the same radial point. Given that, we will restrict the expression radial flight to refer to jumps between trappings or turn over points. In this simplified picture, we consider that the tracers are trapped for a certain time, the trapping time, at a fixed radial position and then they jump to another trapping or to a point where the radial component of the velocity changes direction. So their trajectories can be characterized by the trapping times and the length of the flights. This approximate picture of the tracer motion allows us to construct a model of the particle transport in plasma turbulence from the perspective of the CTRW model.

Two examples of a tracer trajectory are shown in figure 1. The tracer on the left panel is confined during the full length of the calculation, and five different trappings can be identified. The tracer on the right panel is trapped during some time, and then jumps out of the plasma. Horizontal lines indicate the separation between trappings or between trappings and flights. Vertical lines indicate the duration of the trappings.

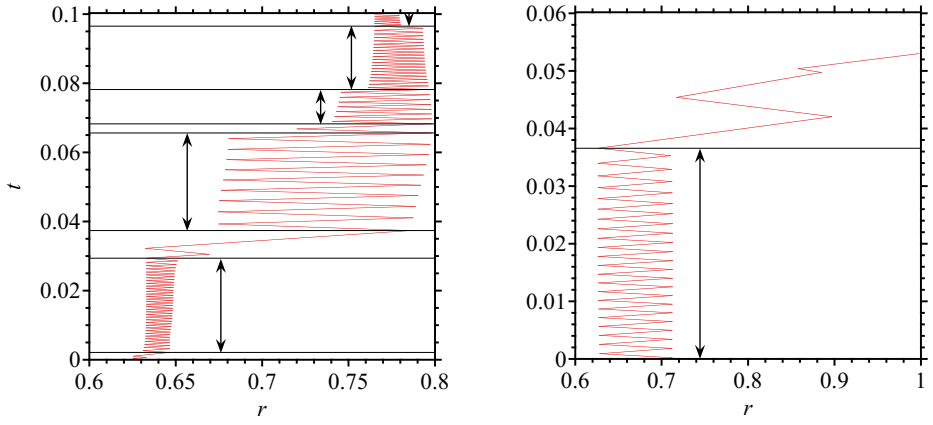

Figure 1. Examples of tracer trajectories. Left: tracer is trapped during the full length of the calculation. Right: tracer leaves the plasma. Vertical lines indicate the duration of the trappings.

fig:tracers

Previously, we have seen the relation between the radial width of trappings and the width of the plasma flow structures [9]. Essentially we saw that the averaged radial displacements during the trappings are directly related to the width of the flow structure, that is the width of the filamentary vortices.

Now we want to characterize the distributions of trapping times so they can be used in a transport model within the CTRW approach. We will begin by following the motion of particle tracers in a fixed turbulent field. This will allow us to establish the relationship between the distribution of trapping times and the topological properties of the turbulent structures, in particular the length of the filaments. Next, we will follow the motion of tracers in an evolving turbulent field. Since the turbulent fields

change over time, the relevant results for the study of transport will be those obtained from the motion of tracers in evolving turbulent fields.

The rest of the paper is organized as follows. The turbulence model used in these calculations is described in section 2. In section 3, we calculate the statistical distributions of trapping times of the tracers for three different configurations, and compare the results with the distribution of filament lengths. In section 4, we study the distribution of trapping times of the tracers when they move in evolving turbulence. A simple probabilistic model for the tracer dynamics is developed in section 5. The conclusions will be presented in section 6.

2. Resistive pressure driven model

sec:PlasmaModel

In this section, we describe the MHD model equations that we use in calculating the turbulent flows generated by resistive pressure-gradient-driven turbulence that are analyzed in this paper. We study the pressure-gradient-driven turbulence in cylindrical and toroidal geometry by means of a reduced set of resistive MHD equations [10] in the electrostatic limit [11]. For most of the cases considered, the geometry is that of a periodic cylinder, with minor radius a and length $L = 2\pi R_0$. If we bend the cylinder in a torus, R_0 is the radius of the axis of the torus. In this section we describe the equations for the toroidal geometry. The changes when we go to the cylindrical geometry are straightforward.

We use a coordinate system (ρ, θ, ζ), in which ρ is either the radius r normalized to a for the cylindrical case, or a radius-like equilibrium flux surface label for the toroidal case, θ is the poloidal angle and ζ is either the toroidal angle for the toroidal case, or $\zeta = z/R$, where z is the coordinate along the axis of the cylinder, for the cylindrical case. The $E \times B$ velocity is written in terms of the electrostatic potential:

$$\mathbf{V}_\perp = -\frac{\nabla \mathbf{\Phi} \times \mathbf{b}}{\mathbf{B}} \tag{1}$$

Vperp

where Φ is the electrostatic potential, $\mathbf{B}$ is the magnetic field, and $\mathbf{b}$ is a unit vector in the direction of the magnetic field.

The model consists of two equations, the perpendicular momentum equation for the electrostatic potential evolution, and the equation of state for the pressure evolution. The first one is

$$m_i n_i \frac{d\tilde{U}}{dt} = -\mathbf{B} \cdot \nabla \left(\frac{R^2}{\eta F^2} \mathbf{B} \cdot \nabla \tilde{\Phi} \right) + 2 \frac{\mathbf{b} \times \boldsymbol{\kappa}}{B} \cdot \nabla \tilde{p} + m_i n_i \hat{\mu} \nabla_\perp^2 \tilde{U} \tag{2}$$

eq:U

Here, $d/dt = \partial/\partial t + \mathbf{V}_\perp \cdot \nabla$ is the convective derivative, $U = \boldsymbol{\zeta} \cdot \nabla \times \mathbf{V}_\perp / B$ is the toroidal component of the vorticity, η is the resistivity, $\boldsymbol{\kappa} = \mathbf{b} \cdot \nabla \mathbf{b}$ is the magnetic field curvature, m_i is the mass of ions, n_i is the ion density, and $\hat{\mu}$ is the viscosity coefficient. The magnetic field is expressed as $\mathbf{B} = F \nabla \zeta + \nabla \zeta \times \nabla \psi$, where $F = R B_\zeta$ is the toroidal flux function and ψ is the poloidal flux. The derivative along the magnetic field can be expressed as

$$\mathbf{B} \cdot \nabla = \frac{F}{R^2} \left(\frac{\partial}{\partial \zeta} - \frac{1}{q} \frac{\partial}{\partial \theta} \right) \tag{3}$$

Bgrad

where q is the safety factor, and R is the major radius. In cylindrical geometry, R and F are constant.

The equation of state for the pressure evolution is

$$\frac{d\tilde{p}}{dt} + \Gamma p \nabla \cdot \mathbf{V}_\perp = D_\perp \nabla_\perp^2 \tilde{p} + D_\parallel \frac{R^2}{F} \mathbf{B} \cdot \nabla \left(\frac{R^2}{F} \mathbf{B} \cdot \nabla \tilde{p} \right) \tag{4}$$

eq:pr

where Γ is the heat capacity ratio.

In equations (2) and (4), a tilde identifies perturbed quantities. For the nonlinear calculations, the effect of the $V_{\|}$ evolution in the dynamics of the resistive pressure-gradient-driven turbulence is replaced by a parallel diffusivity in the pressure equation. Viscosity and perpendicular transport are also included in the equations to provide the energy sink needed to get steady-state turbulence.

The driving term of the resistive pressure driven instability is the pressure gradient in the bad curvature region, that is, the second term on the right-hand side (rhs) of equation (2). The first term on the rhs is the field line bending term, which is stabilising. The resistivity weakens this term and allows the instability to grow.

In equation (2), the viscous term of the rhs for the $(m = 0, n = 0)$ component is a viscous drag $-m_i n_i \mu \tilde{U}_{00}$ due to magnetic pumping. In equation (4), an energy source term is added to the rhs for the $(m = 0, n = 0)$ component in order to compensate for dissipation and maintain a steady state.

Two different magnetic configurations are considered here. The first one is a model of a configuration of the Large Helical Device (LHD) [12] in cylindrical geometry. The second is a toroidal configuration that corresponds to a medium-size tokamak with circular cross section [13]. The turbulent flow is generated by resistive interchange modes in the first configuration, and by ballooning modes in the second configuration. The main difference between the flow structures of both configurations is the presence of streamers in the second one. They are long structures that link the interior of the plasma to the edge by merging many vortex structures. Details of the configurations, numerical methods, and main parameters can be found in Ref. [9].

3. Relation between flow topology and tracer transport

sec:TopolTracers

As we have already described in [2], [3], to study the topological structures of the turbulent flow we work with the electrostatic potential Φ. All the information on the turbulence is contained in the function Φ. For instance, turbulence vortices can be easily identified by looking at the contours of the function Φ. We define a cubical space $N_r \times N_\theta \times N_\zeta$ covering the cylinder. At a fixed time t, we define a flow structure as the set of points such that $\Phi(r, \theta, \zeta, t) \geq \Phi_0 \max(\Phi)$, for a suitable constant Φ_0, with $\max(\Phi)$ being the maximum value Φ at time t. Therefore, Φ_0 gives a fraction of the maximum value of Φ and $0 \leq \Phi_0 \leq 1$.

The main finding of Ref. [2] was that, when no average poloidal flow is present, the structure of the flow is filamentary. The filaments are vortices that are linked to the rational surfaces. The cycles are filamentary vortices that close on themselves forming toroidal knots. They are normally located at the lowest rational surfaces. At the other low rational surfaces the filaments are broken and we characterise them by their length. Probably the most remarkable property that we have observed is the lognormal character of the distribution of filament lengths [2]. When an averaged poloidal flow is included, some new topological structures appear in the shape of a cylindrical shell. They are associated with the transport barriers created by the shear in the mean flow (zonal flows). We call them mini-transport barriers and were discussed in detail in [9].

Having studied the properties of the flow structures, we can now study the statistical properties of the trapping times of tracer particles when they are moving in the same turbulent flow fields.

Using the velocity fields obtained from the resistive pressure-gradient-driven turbulence calculations discussed in [9], we have studied the evolution of tracer

particles. The velocity field perpendicular to the magnetic field is given in terms of the electrostatic potential, $\Phi(\rho, \theta, \zeta, t)$, by equation (1). Then the evolution of the tracers is given by

$$\frac{d\mathbf{r}}{dt} = -\frac{\nabla\Phi \times \mathbf{b}}{B} + V_0\mathbf{b}, \tag{5}$$ eq:tracer

where $\mathbf{r} \equiv (\rho, \theta, \zeta)$ is the tracer position, and V_0 is a constant velocity along the magnetic field lines. In solving this equation we can take Φ at a fixed time and use the frozen field or we can take Φ to be a function of time and then we have a dynamical evolution of tracers. In this section, in order to understand better the relation between flow structures and tracer transport, we will start with the first option.

When we look at tracer particle motion, we see that vortices may cause some of the trapping of particles, while large scale flows may carry them from vortex to vortex. Here we interpret the tracer trajectories from the point of view of the CTRW model. First, we decompose the tracer trajectories in radial flights. As we have explained in the Introduction, a sequence of flights around the same radial point corresponds to a trapping; the rest of flights are jumps either between trappings or out of the plasma. These jumps also can have one or many flights. Precise criteria for trappings are important and far from trivial, since the oscillation of the tracer around a radius, even though regular, may be complicate to separate different trappings as in the case shown in figure 1. We first look for tracers that are trapped during the full length of the calculation. Their trajectories verify a periodicity condition in the whole trajectory. If there is more than a single trapping, we calculate for each local maxima (minima) the averaged radius of the part of the trajectory between that local maxima (minima) and the next one. We define a trapping as a set of consecutive maxima (minima) such that the difference of averaged radius between two successive maxima (minima) is less than 5% of the radial width of the portion of the trajectory defined by the set of maxima (minima). Details on the numerical identification of trappings are given in Ref. [9]. We have done tests of the criteria used, for instance we have joined consecutive trappings with similar averaged radius. All these tests give statistical results that are very close.

For the analysis of the flow structures, we consider 2-D subsets corresponding to ζ = constant. In each of these toroidal cuts, we identify the connected components following the same approach as we did for the radial slices in [2] and we determine the radial extend of each of them. These connected components are the topological flow structures that we discuss here. The trapped tracer trajectories are linked to the flow structures. These structures can correspond to individual vortices, merged vortices or mini-transport barriers associated to zonal flows.

To visualize the topological flow structures and to compare them with the particle tracer orbits, we do first a transformation of the poloidal angle θ to

$$\theta \to \theta + \zeta/q(r) \tag{6}$$ theta1

With this transformation, we unscrew the helical structures in such a way that the magnetic field lines became parallel at the axis of the cylinder. Then we can project the structures on the $\zeta = 0$ plane. We can represent this projection in the plane (r, θ); this will give spots that show the maximum width of the structures on the whole ζ range.

Fig. 2 shows the projected structures in the (r, θ)-plane for the cylindrical configuration and $\Phi_0 = 0.1$. Also it is shown (in blue) the trajectory of a tracer. The tracer is most of the time trapped at different structures and occasionally jumps

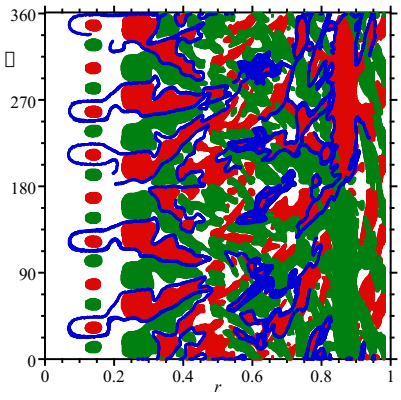

Figure 2. Projection of flow structures. Points for which $\Phi \geq 0.1\max(\Phi)$ are in red and points for which $\Phi \leq -0.1\max(\Phi)$ are in green. The trajectory of a tracer is shown in blue. The apparent discontinuities in the trajectory are due to the transformation (6).

fig:traject

between them.When we draw the orbits with respect to the new variables, there can be discontinuities due to the transformation (6).

Trappings and flights are closely related to the properties of the plasma flow. Radial excursions are relatively regular during the trapping period but they can vary a great deal from trapping to trapping. Previously, we have found a clear correlation between the radial extend of the flow structures and the radial excursions of the tracer particles during their trapping phase [9]. The character of trapping may change with the magnetic field geometry and by the presence of an averaged flow.

In this paper, we focus on the relation between the trapping times and the flow structures for three different plasma configurations [9]. Two of them correspond to a stellarator magnetic configuration. In these cases, the main instability is the resistive interchange mode and they can be modeled in cylindrical geometry. In the first one, no averaged poloidal flow is present, and in the second, the averaged poloidal flow is self-consistently generated by the Reynolds stress. The third configuration corresponds to a tokamak magnetic configuration. In this case the dominant instability is the resistive ballooning mode and it is modeled in toroidal geometry. No averaged poloidal flow is included in this case. We have studied the evolution of tracers for the three configurations and different values of V_0. The initial tracer positions are randomly distributed in the torus, and we follow the trajectory of 10^5 tracers till the end of the calculation and accumulate the data. This data is analyzed to identify the portion of the trajectories that the tracers remain trapped.

For each case, we have two sets of data on the trapping. There is one set for the trappings that do not reach the end of the calculation, that is, a set of data in which the trapping phase is completed. There is another set in which the tracers were still trapped the last step. In this last set we have tracers that have practically only one trapping during the full length of the calculation. The length of the calculation is one resistive time for the stellarator cases, and $0.1\tau_R$ for the tokamak case. The percentage of tracers that have only one trapping during the full length of the calculation is shown in figure 3. The difference between the resistive interchange and ballooning configurations (1 and 3) is due to the presence of streamers in the latter.

In most of the instances, tracers following streamers just leave the plasma. Note that the difference is not between tokamaks and stellarators, but between toroidal and cylindrical geometry instability models. The difference between the interchange case with and without averaged poloidal flow (configurations 2 and 1) is due to the presence of mini-transport barriers in the former. In the case without an averaged poloidal flow, most of the tracers with only one trapping remain trapped in large-scale cycles. When an averaged flow is present, a significant fraction of tracers with only one trapping (around 50% for configuration 2) get trapped in the mini-transport barriers created by the shear of the averaged poloidal flow [9].

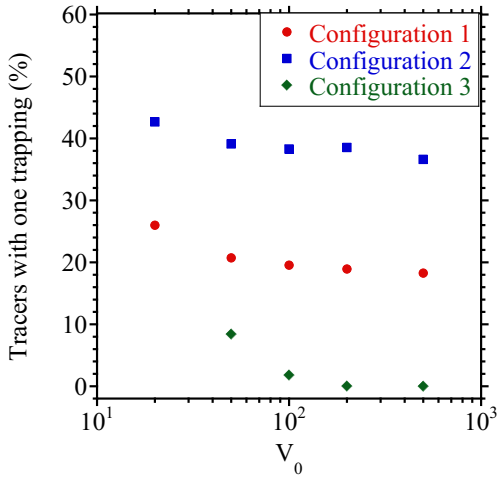

Figure 3. Percentage of tracers that have only one trapping during the full length of the calculation.

fig:onetrap

For the set of data in which the trapping phase is completed, we group the trappings in two different groups. For the first group we select the trappings in flow structures, which are defined as follows: we calculate the pitch q_p of the averaged tracer trajectory in the (θ, ζ) plane and the trapping belongs to the first group if q_p has a value within the interval defined by q at $\langle r\rangle + \langle\Delta r\rangle/2$ and q at $\langle r\rangle - \langle\Delta r\rangle/2$. Here, $\langle r\rangle$ is the mean value of r during the tracer trajectory, and $\langle\Delta r\rangle$ is the mean value of the radial flights of the tracer. In figure 4, we show the percentage of the total trapping time that tracers are trapped in flow structures for the set of data in which the trapping phase is completed. Tracers are trapped most of the time in flow structures for the cases without averaged flow (configurations 1 and 3). The situation is the opposite in the case of averaged flow (configuration 2), where the time spent by the tracers in trappings in the mini-transport barriers dominates the dynamics.

We have calculated the probability distribution function (PDF) of the trapping times for the three configurations and different values of the parallel velocity of the tracers V_0. The results for the group of trappings in the flow structures for configuration 1 are shown in figure 5, at the left. The right panel shows the Rank function for the same cases. The Rank function is defined as 1 minus the cumulative distribution function, and the tail of the Rank function is better defined than the one of the PDF since there is no need to use binning and all points of the sample are points of this function. The distribution of trapping times for each value of V_0 seems

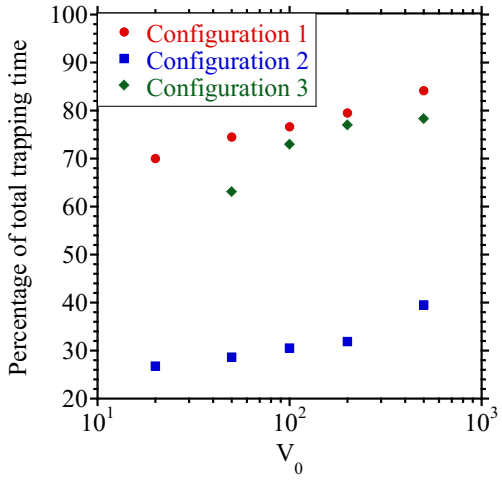

Figure 4. Percentage of the total trapping time that tracers are trapped in flow structures.

fig:flowstr

to be well described by a lognormal distribution

$$p(x) = \frac{1}{x\sigma\sqrt{2\pi}} \exp\left[-\frac{(\ln x - \mu)^2}{2\sigma^2}\right] \tag{7}$$

logn

The corresponding Rank function is

$$R(x) = \frac{1}{2} - \frac{1}{2}\,\mathrm{erf}\left(\frac{\ln x - \mu}{\sqrt{2}\sigma}\right) \tag{8}$$

lognrank

Here, μ an σ are the mean and standard deviation of the trapping time natural logarithm, respectively. In figure 5, at the left, we plot the PDFs of the trapping times together with fits (thick lines) of the Rank function by equation (8) since the Rank function gives a better description of the data.

The mean value of the lognormal distribution as a function of the parallel velocity V_0 is plotted in figure 6. The mean value scales as $1/V_0^{\alpha}$, where the power law decay index α is 0.78. Since α is close to 1, this suggests a possible relationship between the PDF of the trapping times and the PDF of the lengths of the filaments, that also has a lognormal character [2].

The length of a filament was calculated in Ref. [2] as the number of cubes covering the filament in a cubical space $N_r \times N_\theta \times N_\zeta$ covering the cylinder. We can estimate then the trapping length L of the associated filament during a trapping time τ as

$$L = \frac{V_0\tau}{2\pi}\sqrt{N_\zeta^2 + \frac{N_\theta^2}{q_p^2}}, \tag{9}$$

eq:length

where $V_0\tau$ is the toroidal angle spanned by the tracer during the time interval τ, and q_p is the pitch of the averaged tracer trajectory. Figure 7 shows the comparison of the PDF of the lengths of the filaments and the PDF of the estimated trapping lengths for the case $V_0 = 500$. In expression (9), we take $N_\zeta = 300$ and $N_\theta = 600$, as in Ref. [2]. The dependence of the tail of both distribution functions is practically the same, confirming that what we defined as trappings in the flow structures correspond to tracers trapped on broken filaments.

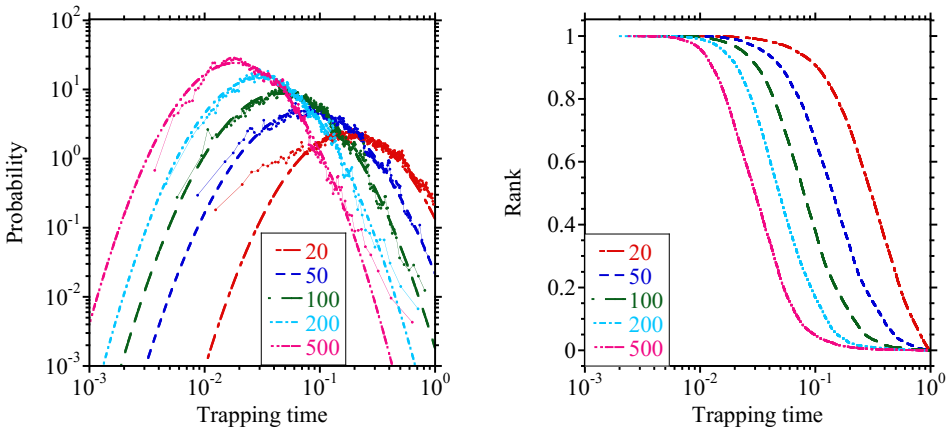

Figure 5. PDF (left) and Rank (right) of the trapping times for configuration 1 and five values of the parallel velocity. Lognormal fits are plotted with thick lines in the left panel.

fig:timesnf

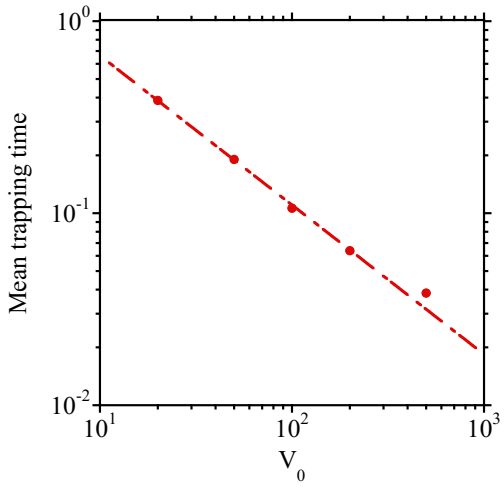

Figure 6. Mean values of the trapping times for configuration 1 and fit to $1/V_0^{\alpha}$ (broken line). The power law decay index α is 0.78.

fig:meannf

The results for the group of trappings in the flow structures for configuration 2 are very similar to configuration 1. Again, the distribution of trapping times for each value of V_0 seems to be well described by a lognormal distribution. The mean trapping time scales as $1/V_0^{\alpha}$, where $\alpha = 0.53$.

However, as we indicated before, the percentage of the total trapping time that tracers are trapped in filaments is less than 40% for configuration 2 (see figure 4). The PDF of the trapping times when tracers are not trapped in filaments is shown in figure 8. The distribution function is practically independent of V_0. This is consistent with the assumption that most of these trappings are in mini-transport barriers. The relation of the radial width of these trappings and the rugosity of the barriers was pointed out in reference [9].

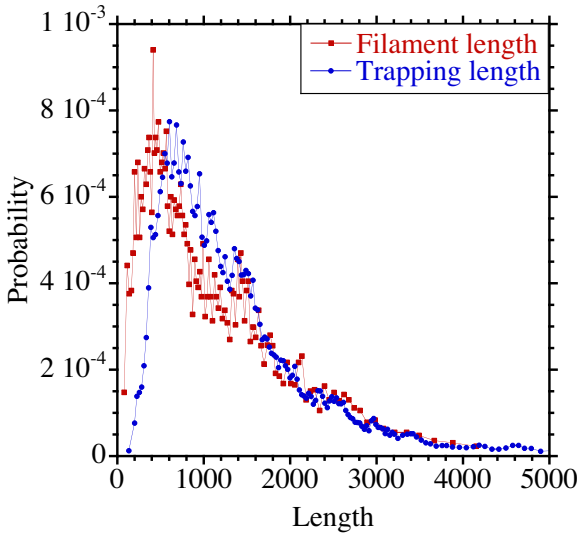

Figure 7. Comparison of the PDF of filament lengths and the PDF of estimated filament lengths during the trapping times for $V_0 = 500$

fig:lengthnf

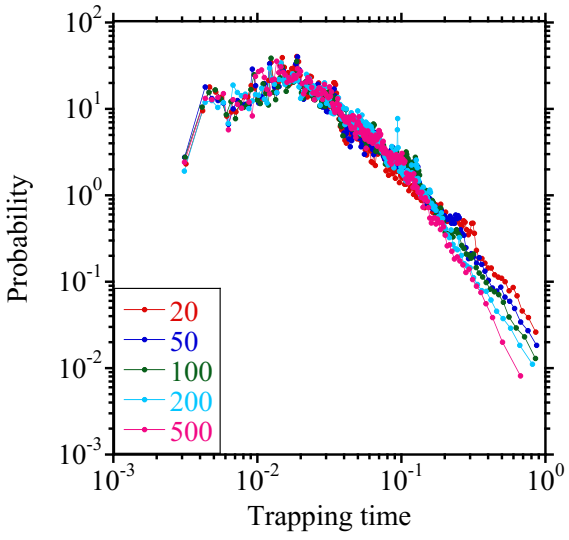

Figure 8. PDFs of the trapping times for configuration 2 and five values of V_0 when tracers are not trapped in filaments.

fig:flowrest

The relative contribution of the two groups of trappings to the PDF of the trapping times can be seen in figure 9. It shows the PDF of trapping times when all the trappings are included, and the contribution to the PDF of the trappings in filaments and of the rest of trappings. The parallel velocity is 500 and panels (a) and (b) correspond to configurations 1 and 2, respectively. The principal contribution in the case without averaged flow (configuration 1) is that of trappings in filaments, and in the case with averaged flow (configuration 2) it is that of trappings in mini-barriers

(rest).

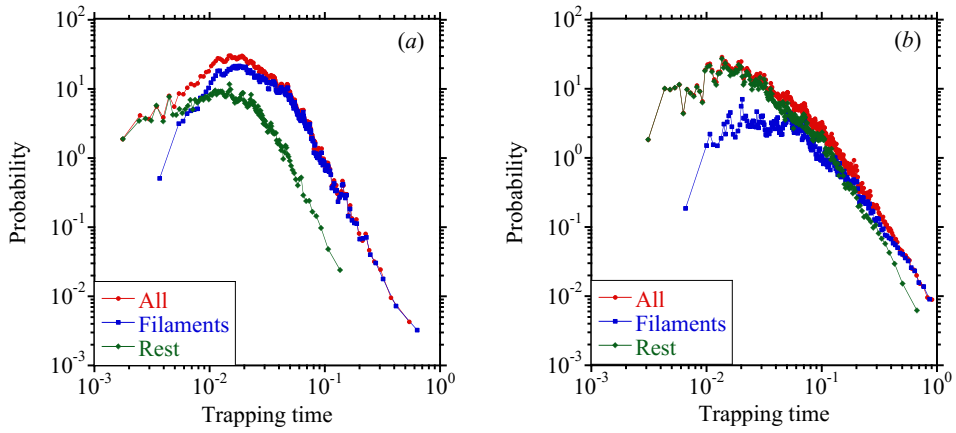

Figure 9. PDF of trappings times for configurations 1 (a) and 2 (b) and $V_0 = 500$. The contributions of trappings in filaments and of the rest of trappings are also shown.

fig:allcyl

The results for the PDF of trapping times in filaments in the case of ballooning modes (configuration 3) also fit to a lognomal distribution, as can be seen in Fig. 10(a) for four values of the parallel velocity. The mean values of the lognomal distribution scale as $1/V_0^{\alpha}$, where $\alpha = 0.87$. The PDF when all trappings are included fit a lognormal distribution again, but the mean values decrease, as can be seen in Fig. 10(b). This is probably due to flights along the streamers.

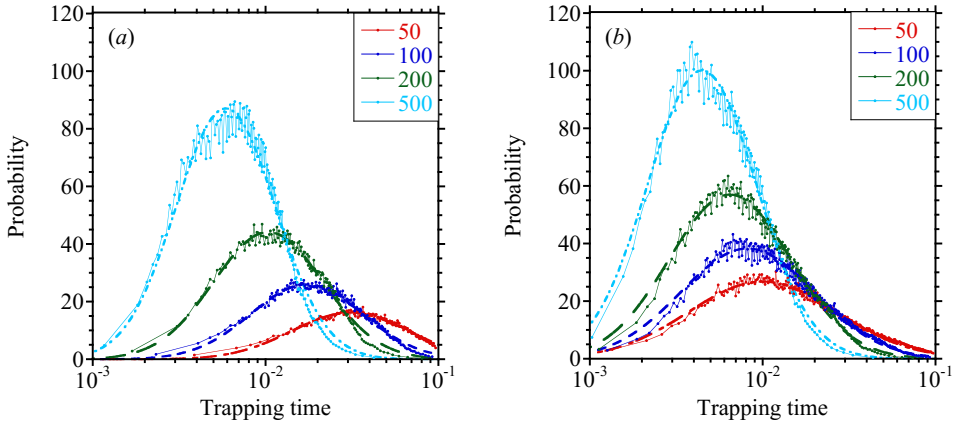

Figure 10. PDFs of the trapping times for configuration 3 and four values of the parallel velocity when only trappings in filaments are included (a), and when all trappings are included (b). Lognormal fits are plotted with thick lines.

fig:timesbal

4. Tracer transport in evolving turbulence

sec:EvolTracers

In the previous section, we have analyzed the trapping of tracers in a frozen turbulent field, now we consider the motion of tracers in a time evolving turbulence field. For the stellarator configurations (configurations 1 and 2), we follow the trajectories of tracers during a time period of $0.8\tau_R$, and for the tokamak configuration (configuration 3) during a period of $0.1\tau_R$. In general, for the evolving turbulence, we have a smoother PDF of the trapping times because of the varying conditions of the flows on one hand and also because during the evolution tracers remain trapped for shorter times and as a consequence the statistics are better than for the case of frozen turbulence.

For the three configurations, the fraction of tracers that have only one trapping during the time interval of the calculation is negligible (0.4% at most). In the previous section, for fixed turbulent fields, the fraction of tracers that had only one trapping during the time interval of the calculation was significant in most cases. This fraction was interpreted to be due to tracers that remained trapped in large-scale cycles or mini-transport barriers. In the case of evolving turbulence, the cycles also evolve in time, and this change is characterized by their life-time. The distribution of life-times for configurations 1 and 3 was calculated in reference [2] and shown in figure 11 of that reference. Since the time interval of the calculation corresponds to many life-times, one expects than only very few tracers will remain in a given cycle.

Filaments also change during the evolution. The change is more difficult to characterize. Filaments can change their length, they can be divided in several new filaments or several fragments can be joined together. Also new filaments can be originated by breaking of the cycles or filaments can be joined in one cycle. For these reasons, to differentiate trappings in filaments is no so clear as in the case of non-evolving turbulence. In spite of this, we will use the same condition for the averaged pitch of the trajectory q_p as we did in the case of non-evolving turbulence to define the trappings in filaments. This characterization of the trapping in filaments becomes less reliable for the short trappings, on the following analysis we will focus on the long trapping times of the PDFs. In figure 11, we show the percentage of the total trapping time that tracers are trapped in filaments. The percentage is much smaller than in the case of non-evolving turbulence, only reaching high values for parallel velocities above 500.

The PDF of the trappings in filaments has a lognormal character and varies with the parallel velocity, although the dependence with V_0 is weaker than in the case of non-evolving turbulence. The large trapping times are now limited by the breaking time of the filaments, as we will discuss in the next section. The results for the stellarator configuration (configurations 1 and 2) are shown in figure 12. The PDFs for both the case with flow and without flow are very similar when $V_0 = 5000$.

When we include all the trappings, the PDFs are practically the same independently of the parallel velocity for each configuration. This is shown in figure 13 for configurations 1 and 2. The PDF in the case without flow is very similar to the one obtained for the trappings in filaments when $V_0 = 5000$. This make sense because for $V_0 = 5000$ almost 80% of the total trapping time was spending in filaments.

In the case of ballooning modes (configuration 3) and evolving turbulence, there are minor variations in the PDFs for the different parallel velocities, as can be seen in figure 14. The comparison of PDFs for evolving and non-evolving fields (configuration 3) is shown in figure 15 for $V_0 = 50$ (panel *a*) and $V_0 = 500$ (panel *b*). The PDFs get closer as the parallel velocity increases.

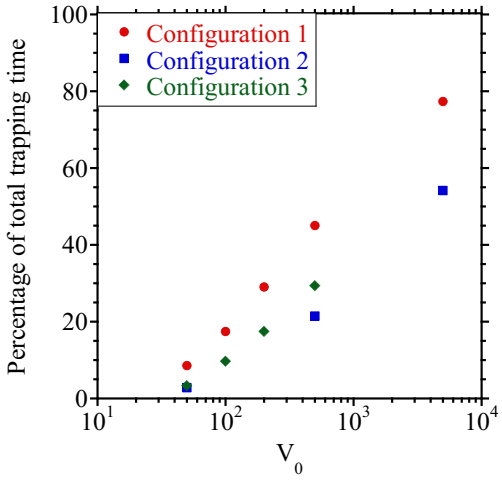

Figure 11. Percentage of the total trapping time that tracers are trapped in filaments in the case of evolving turbulence.

fig:filstr

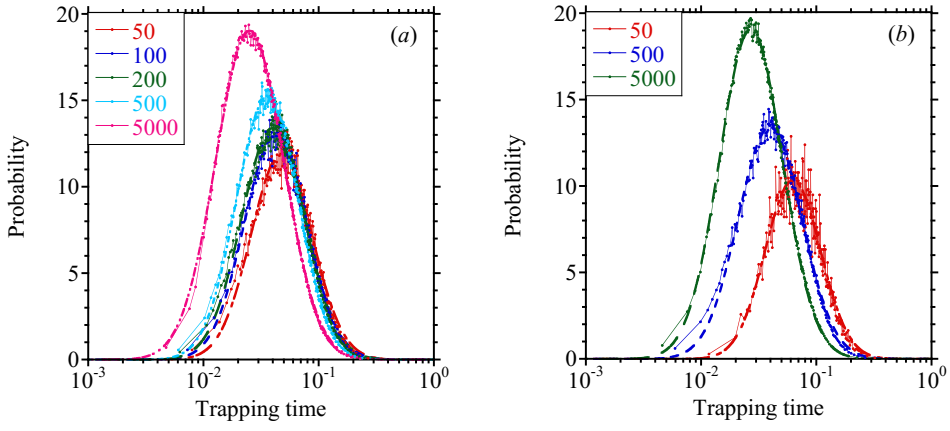

Figure 12. PDFs of the trapping times for configurations 1 (panel a) and 2 (panel b) in the case of evolving turbulence and for trappings in filaments. Labels indicate the value of V_0. Lognormal fits are plotted with thick lines.

fig:cylfildyn

Figure 16 shows the comparison of PDFs for evolving and non-evolving fields for the stellarator case without averaged flow (configuration 1). $V_0 = 50$ in panel a, and $V_0 = 500$ in panel b.

5. Probabilistic model for the tracer dynamics

ec:Trappingmodel

To better interpret the previous results, we have developed a probabilistic model describing the dynamics of the tracers that are trapped on a filament. This model is not expected to give a quantitative detailed description of the tracer dynamics but just a qualitative view of the main mechanisms involved.

The idea of the model is to construct a walk in which each step is $\delta\rho$, that is the radial excursion of the tracer when trapped. In this model we need to define first the

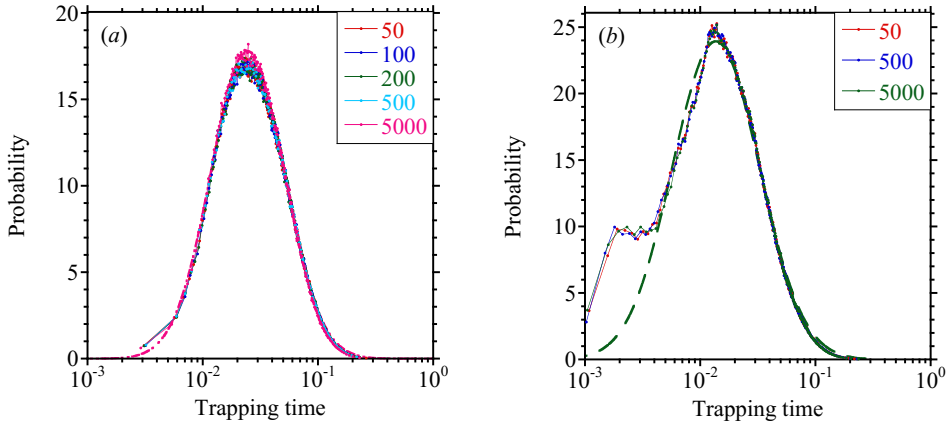

Figure 13. Same as figure 12 when all trappings are included. Lognormal fits correspond to the cases $V_0 = 5000$

fig:cyldyn

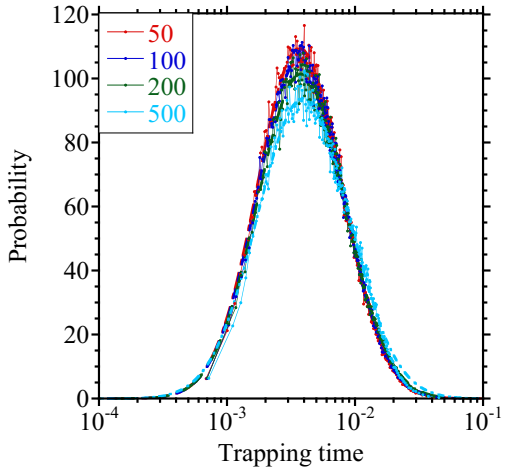

Figure 14. PDFs of the trapping times for configuration 3 in the case of evolving turbulence. Labels indicate the value of V_0. Lognormal fits are plotted with thick lines.

fig:baldyn

initial conditions and then we will give the stepping process. Initial conditions:

(i) $\delta\rho$, the radial step size. From the tracer results we know that the averaged value of $\delta\rho$ during the trapping is approximately lognormal distributed. So we generate a random value from a lognormal distribution

(ii) V_r, the radial velocity. From the tracer results we know also that the averaged value of the radial velocity is approximately normal distributed. So we generate for V_r a random value from a Gaussian distribution.

(iii) L, the length of the filament along which the tracer moves. In Ref. [2] we showed that L is lognormal distributed, so we generate a random value from a lognormal distribution with parameters $\mu = 6$ and $\sigma = 1$ for the stellarator configuration without flow.

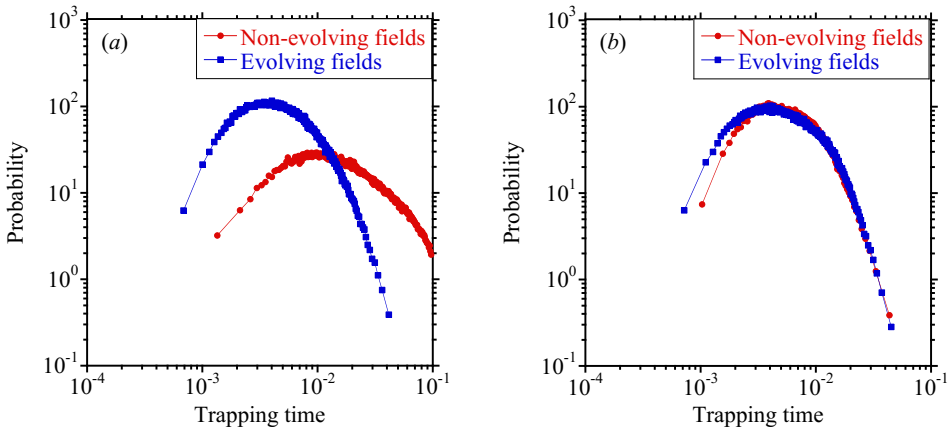

Figure 15. PDFs of trapping times for evolving and non-evolving turbulence (configuration 3) when $V_0 = 50$ (panel *a*) and $V_0 = 500$ (panel *b*)

fig:balfrozdyn

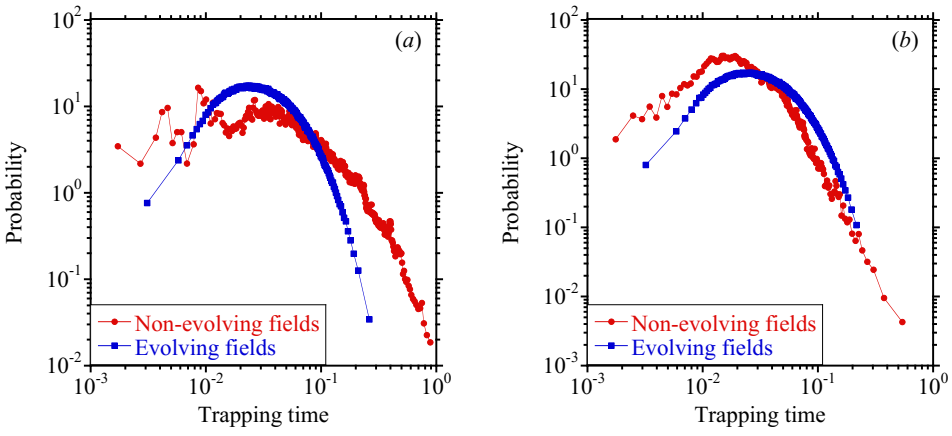

Figure 16. PDFs of trapping times for evolving and non-evolving turbulence (configuration 1) when $V_0 = 50$ (panel *a*) and $V_0 = 500$ (panel *b*)

fig:nffrozdyn

(iv) V_0, the tracer parallel velocity. This is the parameter that we will change to describe the different cases studied previously.

(v) q, the safety factor at the radial point. We choose a random number between 1 and 2 for the stellarator configuration.

From these condition we immediately have that the time of each step is $\Delta t = \delta\rho/V_r$. From step n to $n+1$ the trapping time increases by Δt and the length of the tracer's trajectory along the filament by

$$\Delta L = V_0 \delta t \sqrt{1+q^{-2}} \tag{10}$$

eq:lengthinc

When this length reaches L the walk is finished.

With this model we can generate distributions corresponding to configuration 1. In figure 17(*a*), we compare the PDF for configuration 1 and $V_0 = 500$ with the

corresponding one generated by this model. There is a reasonable agreement between the two.

When we change the parallel velocity (figure 17, panel b), the PDFs show the same type behavior as the ones in figure 5. So the model reproduces the basic features of the numerical results.

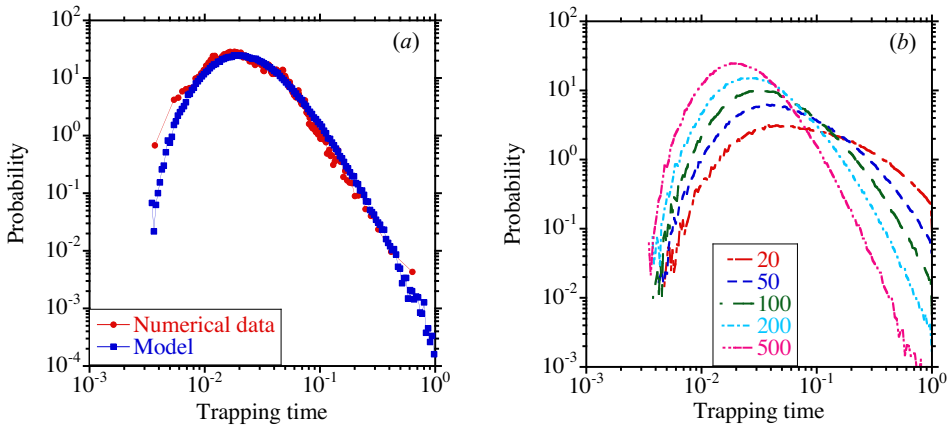

Figure 17. Comparison of the PDF of trapping times of configuration 1 and of the model when $V_0 = 500$ (panel a). PDF of trapping times of the model for five values of V_0 (panel b)

fig:nfmodel

If we now consider the case of the time evolving turbulence the model must be changed to include two effects:

(i) The length of the broken filaments may change with time, so we include a probability p_1 of the tracer to be detrapped during the walk.

(ii) In the non-evolving case, tracer trapped on a cycle did not contribute to the PDF of the trappings because they remain trapped for ever. However, in the evolving case, cycles break and tracers can be detrapped. So we introduce a probability p_0 for a tracer to be on a cycle and a probability p_2 to be detrapped.

These two effects modify the structure of the PDF of the trappings. In this case of evolving fields the agreement between the model and numerical results is not as good as in the non-evolving case but still the model give some of the qualitative features. In figure 18(a), we compare the PDF for the time evolving configuration 1 and $V_0 = 500$ with the corresponding one generated by this model.

When we change the parallel velocity (figure 18 panel b), the PDFs show a similar type behavior as the ones in figure 12(a). So the model reproduces the basic features of the numerical results. Only the case with $V_0 = 5000$ shows a bit of discrepancy.

In comparing the evolving and non-evolving results, the model shows the same feature illustrated for the numerical results in figure 16. In this figure and for $V_0 = 500$, we see that for a certain range of values of the longer trapping times, the PDF for the evolving fields gives higher probability than the one for non evolving fields. At first sight, this result does not seem to make much sense. For the model and in figure 19, we plotted the PDFs for the same velocities than in figure 16 and we can see the same behavior.

In the model we can understand the reason for this behavior. The higher probability for longer trapping times in the case $V_0 = 500$ comes from the contribution

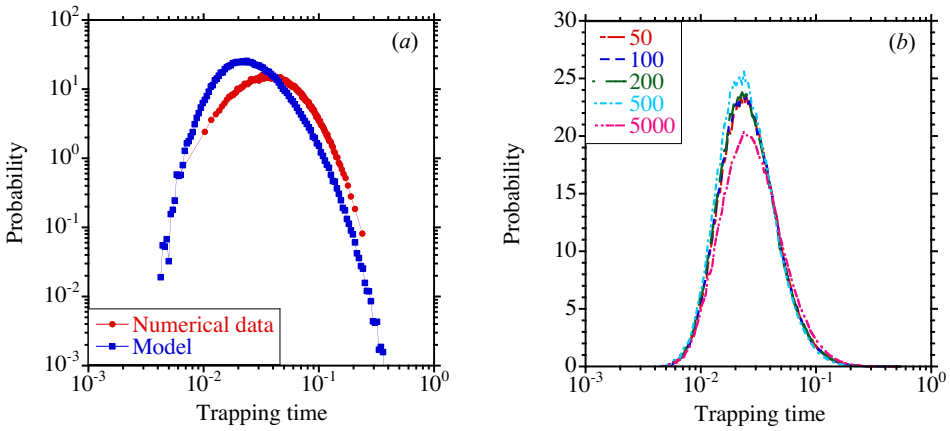

Figure 18. Comparison of the PDF of trapping times of configuration 1 and of the model when $V_0 = 500$ (panel *a*) in the case of evolving fields. PDF of trapping times of the model for five values of V_0 (panel *b*)

fig:dynmodel

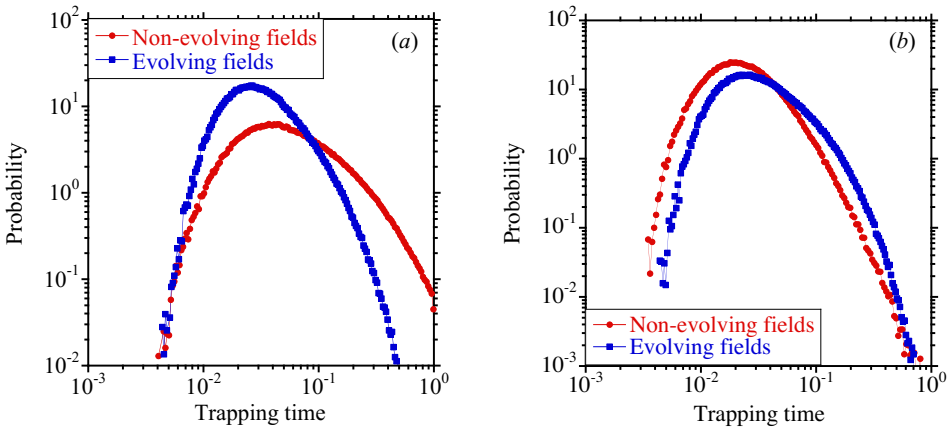

Figure 19. PDFs of trapping times from the model for evolving and non-evolving turbulence when $V_0 = 50$ (panel *a*) and $V_0 = 500$ (panel *b*)

fig:frzdynmodel

of the trapping on the cycles, which did not contribute in the non-evolving case. This contribution becomes more significant at higher velocities, above 100 in our case. If the contribution of the tracers trapped on cycles is not included the effect shown for $V_0 = 500$ will not appear.

This simple probabilistic model is useful in understanding the changes from the statical case to the dynamical in the configuration 1. For the tokamak configuration the process is more complicated. Tracers jump from one filament to another in the streamer region, also in this region there are losses. Therefore the trajectories do not remain on a fixed radius and the simple model given here cannot be applied.

sec:Conclusions

6. Conclusions

We have studied the trapping of passive tracers in a turbulent field for three different plasma configurations. Two of them correspond to a stellarator magnetic configuration. In the first one, no averaged poloidal flow is present, and in the second, the averaged poloidal flow is self-consistently generated by the Reynolds stress. For these configurations the main instability is the resistive interchange mode. The third configuration corresponds to a tokamak magnetic configuration. In this case the dominant instability is the resistive ballooning mode.

For the configuration without averaged flow, most tracers are trapped on vortex filaments. Most of the tracers trapped at the end of the calculation are trapped on closed vortex filaments, cycles, the other ones are mostly trapped in broken filaments. Most of these tracers show multiple trappings.

In the case of stellarator configurations, the fraction of passive tracers that remain trapped for long times, longer than the calculation time, is large, whereas the fraction is very small in the tokamak configuration. This is due to the presence of streamers in the latter. In the stellarator case without averaged flow, most of the tracers with only one trapping remain trapped in large-scale cycles. When an averaged flow is present, a significant fraction is trapped in the mini-transport barriers associated to the zonal flows.

The most important conclusion of this paper is that the trapping time of the passive tracers in flow structures follows a lognormal distribution. When the configuration is not dynamically evolving the parameters of the distribution depend strongly on the parallel velocity of the tracers and the distribution is related to the PDF of filament lengths. In the case of evolving turbulence, the dependence of the PDF of trapping times on the parallel velocity is weak. This is another important conclusion in order construct a transport model based on CTRW.

For configurations 1 and 2, some of the features of the tracer dynamics can be explain with a simple probabilistic model. The distributions generated by the model show good agreement with the ones obtained from the tracers. Because of the more complicated dynamics, in the tokamak case with evolving fields the simple model cannot be applied.

Acknowledgments

This research was sponsored by DGICYT (Dirección General de Investigación Científica y Técnica) of Spain under Project No. ENE2015-68265-P.

References

Doyle [1] E J Doyle et al. Progress in the ITER Physics Basis Chapter 2: Plasma confinement and transport 2007 *Nucl. Fusion* **47** S18

Carreras3 [2] B. A. Carreras, I. Llerena and L. García, *J. Phys. A: Math. Theor.* **46**, 375501 (2013)

Carreras5 [3] B.A. Carreras, I. Llerena Rodríguez and L. García, *Nucl. Fusion* **54** 103005 (2014)

Montroll [4] E. W. Montroll and G. Weiss, *J. Math. Phys.* **6**, 167 (1965)

Vlad [5] Vlad M., Spineanu F., Misguich J.H. and Balescu R. 2002 *Nucl. Fusion* **42** 157

Basu [6] Basu R., Jessen T., Naulin V. and Rasmussen J.J. 2003 *Phys. Plasmas* **10** 2696

Hauff [7] Hauff T. and Jenko F. 2007 *Phys. Plasmas* **14** 092301

Carreras2 [8] Carreras B.A., Lynch V.E. and Zaslavsky G.M. 2001 *Phys. Plasmas* **8** 5096

Garcia1 [9] L. García, I. Llerena Rodríguez and B.A. Carreras, *Nucl. Fusion* **55** 113023 (2015)

Strauss [10] H.R. Strauss, *Phys. Fluids* **20**, 1354 (1977)

Garcia2 [11] L. Garcia, B.A. Carreras and V.E. Lynch, *Phys. Plasmas* **6**, 107 (1999)
Iiyoshi [12] A. Iiyoshi, et al., *Nucl. Fusion* **39**, 1245 (1999)
Garcia3 [13] L. Garcia, and B.A. Carreras, *Phys. Plasmas* **13**, 022310 (2006)